Silver nano particle formation on Ar plasma – treated cinnamyl alcohol

S. Dahle, M. Marschewski, L. Wegewitz, W. Viöl, and W. Maus-Friedrichs

Citation: Journal of Applied Physics **111**, 034902 (2012); doi: 10.1063/1.3680883
View online: http://dx.doi.org/10.1063/1.3680883
View Table of Contents: http://scitation.aip.org/content/aip/journal/jap/111/3?ver=pdfcov
Published by the AIP Publishing

Silver nano particle formation on Ar plasma – treated cinnamyl alcohol

S. Dahle,[1,2] M. Marschewski,[1] L. Wegewitz,[1,3] W. Viöl,[2] and W. Maus-Friedrichs[1,3,a)]
[1]*Institut für Physik und Physikalische Technologien, Technische Universität Clausthal, Leibnizstrasse 4, 38678 Clausthal-Zellerfeld, Germany*
[2]*Hochschule für Angewandte Wissenschaft und Kunst, Fakultät für Naturwissenschaften und Technik, Von-Ossietzky-Straße 99, 37085 Göttingen, Germany*
[3]*Clausthaler Zentrum für Materialtechnik, Technische Universität Clausthal, Leibnizstrasse 4, 38678 Clausthal-Zellerfeld, Germany*

(Received 24 October 2011; accepted 4 January 2012; published online 3 February 2012)

Metastable induced electron spectroscopy, ultraviolet photoelectron spectroscopy, X-ray photoelectron spectroscopy, and atomic force microscopy are employed to study the adsorption of silver on cinnamyl alcohol films prepared on Au(111) substrates by thermal evaporation. Additionally, the impact of an Ar atmosphere dielectric barrier discharge plasma applied to the cinnamyl alcohol film preliminary to the Ag adsorption is investigated. In both cases silver nano particles with an average diameter of 9 nm are formed. These particles do not interact chemically with the underlying cinnamyl alcohol film. We do not find any influence of the preliminary Ar plasma-treatment on the adsorption behavior at all. © *2012 American Institute of Physics*. [doi:10.1063/1.3680883]

I. INTRODUCTION

The adsorption of silver on different organic substrates is of great technological interest for various applications, such as corrosion protection, RF shielding, reflective coatings, and many more. Over the past 20 years, especially silver nano particle coatings drastically increased in importance, due to their outstanding functionality. For instance, silver nano particles are known to enhance the efficiency of organic light emitting devices,[1] whereas silver films on TiO_2 nano particles enhance photocatalytic reaction rates.[2,3] One of the most common applications of silver particles is the functionalization of surfaces because of their antibacterial properties.[4,5] This may be useful especially on wood surfaces to preserve them from aging through attack of microorganisms by other means than lacquering or impregnation.

The relevance of surface modifications of wood by means of laser or plasma technology increased substantially in the past few years.[6–18] Low-temperature radio frequency plasma treatment is found to enhance the durability of nano particle coatings.[5] Therefore, a combined method of plasma-treatment and metal nano particle coating may be quite interesting for industrial applications regarding economical aspects as well as an improvement of functionality. The combination of both surface treatments is possible in numerous ways, e.g. by using a plasma-jet with precursor gases.[19,20] To understand the interaction with wood surfaces, several molecular precursors are used to resemble the organic groups of lignin and cellulose. For lignin (see Fig. 1(a)), these precursors are sinapyl alcohol (see Fig. 1(b)) and coniferyl alcohol (see Fig. 1(c)) as two main monolignols, which form lignin. Since these two are derived from cinnamyl alcohol (also known as phenylallyl alcohol, see Fig. 1(d)), we use this less complex molecule as the main lignin precursor for our investigations presented here.[21–23] The effect of plasma treatments on the discussed molecules has been studied previously.[24] In the course of that work, a significant decrease of carbon-oxygen single bonds was observed subsequent to plasma treatments in argon. Along with the accumulation of carbon that is not bound to oxygen, this indicates a reduction of the molecules at the surface. The fraction of carbon-oxygen double bonds almost does not change.[24]

In this study, first results of the adsorption behavior of silver on thin pure and Ar plasma treated cinnamyl alcohol films are presented. These results are part of a research project concerning the interaction of metals (Ag, Ti) with wood surfaces particularly with regard to a preliminary plasma treatment. Cinnamyl alcohol serves as the main precursor. Basing on these results we will improve the understanding of such complex systems as wood. The final aim is to render a combined functionalization by plasma treatment and metal coating in one process step.

Further reactions with atmospheric gases as well as typical volatile organic compounds will be addressed in the following publications. These may be of technological interest especially for cinnamyl alcohol, since it is not only precursor to lignin, but also very popular as an ingredient in various cosmetic products as perfumes, deodorants, or oils.[25,26] Unfortunately, many people experience allergic reactions through contact with cinnamyl alcohol.[27,28] Thus, any interaction that may be able to reduce this allergen in cosmetic products is of great technological interest.

II. EXPERIMENTAL DETAILS

An ultra high vacuum (UHV) apparatus with a base pressure of 5×10^{-11} hPa, which has been described in detail previously,[22,29–32] is used to carry out the experiments. All measurements were performed at room temperature.

a)Author to whom correspondence should be addressed. Electronic mail: w.maus-friedrichs@pe.tu-clausthal.de.

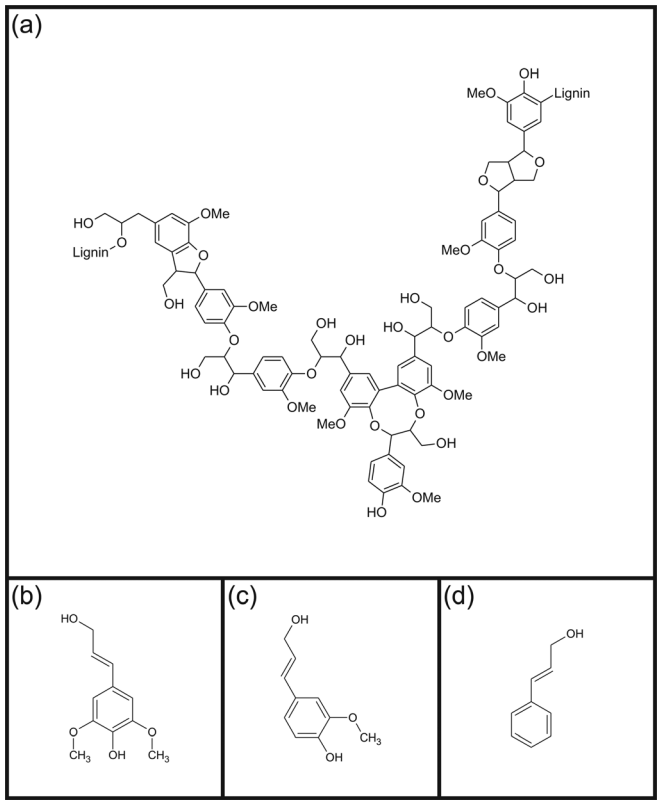

FIG. 1. Chemical structure of lignin (a) and the three main precursors sinapyl alcohol (b), coniferyl alcohol (c), and cinnamyl alcohol (d).

Electron spectroscopy is performed using a hemispherical analyzer (Leybold EA 10) in combination with a source for metastable helium atoms (mainly He* $^3S_1$) and ultraviolet photons (HeI line). A commercial non-monochromatic X-ray source (Fisons XR3E2-324) is utilized for X-ray photoelectron spectroscopy (XPS).

During XPS, X-ray photons hit the surface under an angle of 80° to the surface normal, illuminating a spot of several mm in diameter. For all measurements presented here, the Al K_α line with a photon energy of 1486.6 eV is used. Electrons are recorded by the hemispherical analyzer with an energy resolution of 1.1 eV for detail spectra and 2.2 eV for survey spectra, respectively, under an angle of 10° to the surface normal. All XPS spectra are displayed as a function of binding energy with respect to the Fermi level.

For quantitative XPS analysis, photoelectron peak areas are calculated via mathematical fitting with Gauss-type profiles using OriginPro 7 G including the PFM fitting module, which applies Levenberg-Marquardt algorithms to achieve the best agreement between experimental data and fit. To optimize our fitting procedure, Voigt-profiles have been applied to various oxidic and metallic systems but for most systems the Lorentzian contribution converges to 0. Therefore, all XPS peaks are fitted with Gaussian shapes. Photoelectric cross sections as calculated by Scofield[33] with asymmetry factors following[34,35] and inelastic mean free paths from the NIST database[36] (using the database of Tanuma, Powell, and Penn for elementary contributions and the TPP-2 M equation for molecules) as well as the energy dependent transmission function of our hemispherical analyzer are taken into account when calculating the stoichiometries. According to Ref. 23, the detail spectra of the C 1s region are analyzed by fitting single Gaussians of equal width for every chemical species. It is assumed to be composed of contributions from carbon-carbon or carbon-hydrogen bonds (C_0), carbon-oxygen bonds (C_1), carbon linked to two oxygen atoms or twice to one oxygen atom (C_2), and a shake-up feature (C^*). For all spectra, no contribution of carboxyl groups were found. The relative positions, i.e., binding energy differences are defined as 1.5 eV for C_0-C_1, 2.9 eV for C_0-C_2, and 6.5 eV for C_0-C^*.

Metastable induced electron spectroscopy (MIES) and ultraviolet photoelectron spectroscopy (UPS) are performed applying a cold cathode gas discharge via a two-stage pumping system. A time-of-flight technique is employed to separate electrons emitted by He* (MIES) from those caused by HeI (UPS) interaction with the surface. The combined He*/HeI beam strikes the sample surface under an angle of 45° to the surface normal and illuminates a spot of approximately 2 mm in diameter. The spectra are recorded simultaneously by the hemispherical analyzer with an energy resolution of 220 meV under normal emission within 140 s.

MIES is an extremely surface sensitive technique probing solely the outermost layer of the sample, because the He* atoms interact with the surface typically 0.3 to 0.5 nm in front of it. This may occur via a number of different mechanisms depending on surface electronic structure and work function, as is described in detail elsewhere.[37–39] Only the processes relevant for the spectra presented here shall be discussed shortly.

During Auger deexcitation (AD), an electron from the sample fills the 1s orbital of the impinging He*. Simultaneously, the He 2s electron carrying the excess energy is emitted. The resulting spectra reflect the surface density of states (SDOS) directly. AD-MIES and UPS can be compared and allow a distinction between surface and bulk effects. AD takes place for all systems shown here.

On pure and partly oxidized metal surfaces with a work function beyond about 3.5 eV, Auger neutralization (AN) occurs as long as the surface shows metallic behavior. As a result the impinging He* atom is ionized in the vicinity of the surface by resonant transfer (RT) of its 2s electron in unoccupied metallic surface states. Afterwards, the remaining He^+ ion is neutralized by a surface electron thus emitting a second surface electron carrying the excess energy. The observed electron spectrum is rather structureless and originates from a self-convolution of the surface density of states.

All MIES and UPS spectra are displayed as a function of the electron binding energy with respect to the Fermi level, thus being able to compare MIES and UPS spectra more easily. Obviously, the binding energy scale is only valid for the AD process. Nevertheless, all spectra including structures originating in the AN process have also been displayed in this particular manner. The surface work function can be determined from the high binding energy onset of the MIES or the UPS spectra with an accuracy of ± 0.1 eV.

Atomic force microscopy (AFM) is applied to study the surface topography and determine the size of the silver nano particles. A Veeco Dimension 3100 SPM is employed to

perform the AFM measurements in tapping mode. Silicon cantilevers (NSC15 with Al backside coating from Micromasch) with a resonance frequency of about 308 kHz and a spring constant of about 40 N/m were used together with an optical lever detection technique. All images were gained with a line-scan frequency of 1 Hz with 512 pixels for each of the 512 lines.

The experiments on cinnamyl alcohol were carried out on inert Au(111) substrates. These substrates have been cleaned prior to the experiments by Ar-sputtering at 4 kV for 20 min and subsequent heating up to 1000 K. The Ag reference was prepared by adsorption on a Si(100) substrate, which was preliminary cleaned by flashing up to 1400 K.

Silver (Sigma-Aldrich, 99%) was evaporated with a commercial UHV evaporator (Omicron EFM3) onto the samples. On a clean Si(100) target metallic silver films grow at a rate of 0.23 nm min^{-1} at room temperature when evaporated with an Ag^+ ion flux of 1 μA at the fluxmeter of the EFM3. This flux is a degree for the number of Ag atoms moving toward the sample per second. The film growth rate for Ag has been estimated from the Si 2p peak attenuation in XPS.

Cinnamyl alcohol (Sigma-Aldrich Co., $>$ 97.0%) was evaporated in a directly connected preparation chamber (base pressure $<10^{-9}$ hPa) using a temperature controlled evaporator (Kentax TCE-BS). During all experiments cinnamyl alcohol has been evaporated at 40 °C for 5 min, leading to a film with a thickness of about 1.8 nm estimated from the Au 4f peak attenuation in XPS.[22]

Plasma treatments have been carried out employing a dielectric barrier discharge. The plasma source is mounted to the preparation chamber mentioned above and has been described elsewhere.[40] An alternating high voltage pulse generator with a pulse duration of $t_p = 0.6\ \mu s$ and a pulse repetition rate of 10 kHz is connected to the dielectric isolated electrode, while the sample forms the grounded counter electrode. The discharge gap is set to about d = 1 mm. During the plasma treatment, a voltage of U = 11 kV (peak) is measured. The high voltage supply delivers a power of P = 2 W. The increase of the sample temperature during the plasma treatment does not exceed 10 K.[41]

Ar (Linde Gas, 99.999%), O_2 (Linde Gas, 99.995%), and H_2O (de-ionized) are offered via backfilling the chamber using a backable leak valve. The gas line is evacuated and can be heated in order to ensure cleanness. A quadrupole mass spectrometer (Balzers QMG311 equipped with a Balzers QMA 140) is used to monitor the partial pressure of the reactive gases simultaneously during all MIES and UPS measurements.

III. RESULTS AND DISCUSSION

In this section, we present our results for the adsorption of silver on cinnamyl alcohol preliminary evaporated onto an Au(111) surface. As described in Sec. II, cinnamyl alcohol films are prepared with thicknesses of about 1.8 nm. Furthermore, we compare these to the results for a similar sample that has been plasma-treated in Ar prior to silver adsorption (as described in Sec. II). As a reference for our interpretation, we also show spectra of a silver film with a thickness of 1.8 nm corresponding to 9 monolayers (ML) on a Si(100) substrate. This thickness was calculated from the attenuation of the Si $2p_{3/2}$ peak in XPS by the adsorbates.[39] For better comprehensibility, results and discussions are divided into two parts, the spectroscopic and the microscopic results.

A. Spectroscopic results

Figure 2 shows MIES (a) and UPS (b) spectra of about 1.8 nm of pure cinnamyl alcohol on Au(111) (red solid lines), 9 monolayer equivalents (MLE) Ag on this cinnamyl alcohol film on Au(111) (black solid lines), 9 MLE Ag on Ar

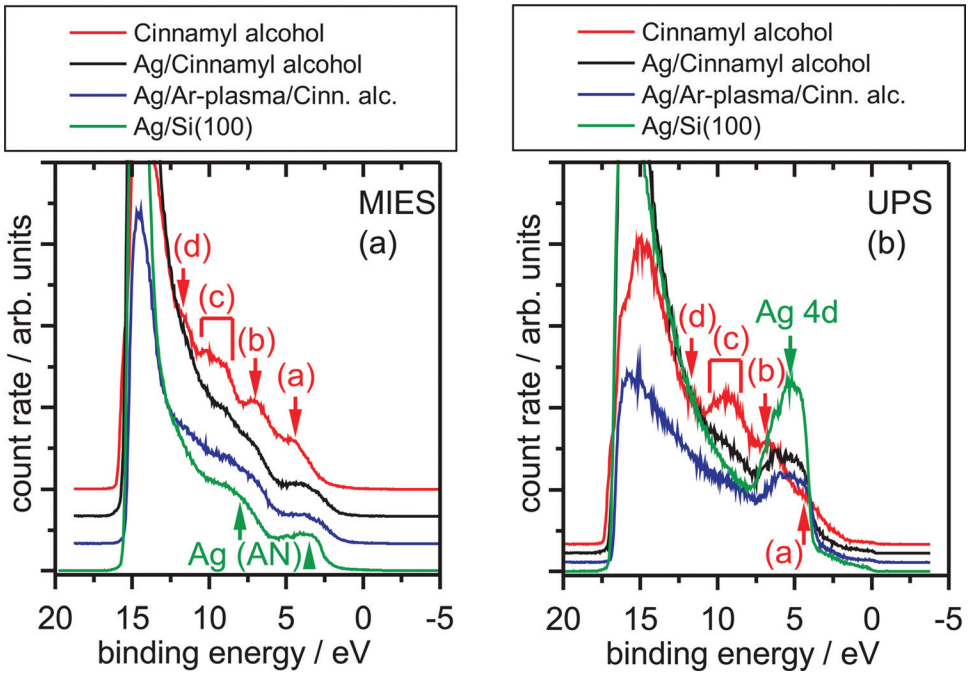

FIG. 2. (Color) MIES (a) and UPS (b) spectra of pure cinnamyl alcohol on Au(111) (red solid lines), Ag on cinnamyl alcohol on Au(111) (black solid lines), Ag on Ar – plasma-treated cinnamyl alcohol on Au(111) (blue solid lines), and Ag on Si(100) (green solid lines).

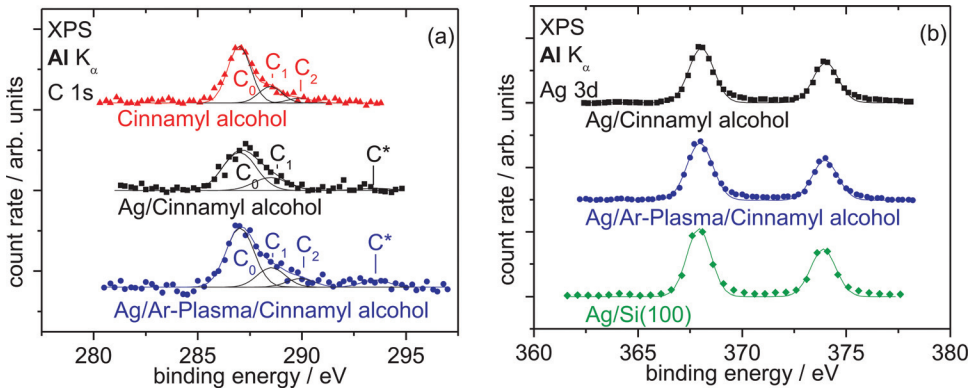

FIG. 3. (Color) XPS spectra of the C 1s (a) and Ag 3d (b) region of pure cinnamyl alcohol (red triangles), Ag on cinnamyl alcohol (black squares), Ag on Ar – plasma-treated cinnamyl alcohol (blue circles), and Ag on Si(100) (green diamonds).

– plasma-treated cinnamyl alcohol with a thickness of about 1.8 nm on Au(111) (blue solid lines), and 9 ML Ag on Si(100) (green solid lines).

All spectra of cinnamyl alcohol show four characteristic spectral features. Feature (a) at a binding energy around 4.4 eV, feature (b) at 7.0 eV, feature (c) from 8.5 to 10.5 eV, and feature (d) at 11.7 eV. These features can be assigned to the molecular orbitals $1e_{1\,g}$ (π) (a); $3e_{2\,g}$ (σCH) and $1a_{2u}$ (π) (b); $3e_{1u}$ (σCH), $1b_{2u}$ (σCC), and $2b_{1u}$(σCH) (c); and $3a_{1\,g}$ (σCH) (d).

Silver on silicon (green line) shows a distinct feature in MIES at a binding energy of 2.8 eV due to the AN process involving two electrons from the 5s orbital.[42] At the lower binding energy side of the secondary electron peak, a broad structure around 7 eV is visible, which is caused by the AN process including electrons arising from Ag 4d and 5s.[42] In UPS, only one peak around 7 eV is visible due to the Ag 4d emission.

For both multilayer samples with Ag on cinnamyl alcohol, MIES shows exactly the same structures as for the pure silver, i.e., only the AN features of Ag are visible. In contrast to that, small contributions of the cinnamyl structures remain in UPS, even though the Ag 4d emission prevails. Since UPS has an information depth of several monolayers, whereas the one for MIES is restricted to the very outermost orbitals of the top layer, this could lead to the conclusion that the surface is covered by a thin film of silver. For all systems we find the AN process in MIES after Ag adsorption. This process is only possible on metallic surfaces with high work functions, hence the adsorbed silver atoms seem to remain metallic. They do probably not form chemical bonds with the cinnamyl alcohol. Even the Ar plasma treatment of the cinnamyl alcohol preliminary to Ag adsorption seems to be without influence on the adsorption behavior.

Figure 3 shows XPS spectra of the C 1s (a) and Ag 3d (b) regions for 1.8 nm of pure cinnamyl alcohol on Au(111) (red triangles), 9 MLE Ag on this cinnamyl alcohol film on Au(111) (black squares), 9 MLE Ag on Ar – plasma-treated cinnamyl alcohol (blue circles), and 9 ML Ag on Si(100) (green diamonds). The original data are shown as point diagrams. The single Gaussians are displayed as solid black line (the fit procedure is described in Sec. II in detail), while the total fit as sum of all Gaussians is displayed as solid line, colored according to the original data. All parameters of the Gaussians are summarized in Tables I for the C 1s region and Table III for the Ag 3d region to achieve better comparability. The binding energies have been normalized so that C_0 in the C 1s has a binding energy of 285.0 eV for all cinnamyl films and Si 2p has a binding energy of 101.7 eV for the reference sample. The composition of the C 1s structure of the cinnamyl alcohol film slightly varies due to relatively high pressures of about 1×10^{-1} hPa during different thermal evaporation procedures. Therefore, a separate table is shown for each experimental series to allow the discussion of every single step. Table I shows C 1s results for experimental series (I), including preparation of cinnamyl alcohol and subsequent Ag adsorption. Table II shows results for series (II),

TABLE I. Summarized XPS results for the C 1s region of experimental series (I).

	Energy	FWHM	Species	Relative intensity
Cinnamyl alcohol	285.0 eV	1.90 eV	C_0	78%
	286.5 eV	1.90 eV	C_1	11%
	287.9 eV	1.90 eV	C_2	9%
	291.5 eV	1.90 eV	C*	2%
Ag/Cinnamyl alcohol	285.0 eV	1.92 eV	C_0	71%
	286.5 eV	1.92 eV	C_1	24%
	287.9 eV	1.92 eV	C_2	0%
	291.5 eV	1.92 eV	C*	4%

TABLE II. Summarized XPS results for the C 1s region of experimental series (II).

	Energy	FWHM	Species	Relative intensity
Cinnamyl alcohol	285.0 eV	1.30 eV	C_0	73%
	286.5 eV	1.30 eV	C_1	21%
	287.9 eV	1.30 eV	C_2	6%
	291.5 eV	1.30 eV	C*	0%
Ar-plasma/cinnamyl alcohol	285.0 eV	1.43 eV	C_0	76%
	286.5 eV	1.43 eV	C_1	19%
	287.9 eV	1.43 eV	C_2	6%
	291.5 eV	1.43 eV	C*	0%
Ag/Ar-plasma/cinnamyl alcohol	285.0 eV	1.58 eV	C_0	63%
	286.5 eV	1.58 eV	C_1	21%
	287.9 eV	1.58 eV	C_2	9%
	291.5 eV	1.58 eV	C*	8%

TABLE III. Summarized XPS results for the Ag 3d region.

	Energy	FWHM	Species	Relative intensity
Ag/cinnamyl alcohol	368.9 eV	1.42 eV	Ag $3d_{5/2}$	50%
	374.9 eV	1.42 eV	Ag $3d_{3/2}$	50%
Ag/Ar-plasma/cinnamyl alcohol	369.3 eV	1.47 eV	Ag $3d_{5/2}$	50%
	375.3 eV	1.47 eV	Ag $3d_{3/2}$	50%
Ag/Si(100)	369.1 eV	1.46 eV	Ag $3d_{5/2}$	58%
	375.1 eV	1.46 eV	Ag $3d_{3/2}$	42%

including preparation of cinnamyl alcohol, Ar plasma treatment, and subsequent Ag adsorption.

The C 1s spectra (a) are composed of four different peaks, corresponding to the chemical species of carbon without any bond to oxygen (C_0), with a single oxygen bond (C_1), with oxygen double bonds (C_2), as well as a shake-up feature due to plasmon excitation (C^*).[23] The ideal stoichiometry for pure cinnamyl alcohol should only show C_1 and 8 times as much C_0. During our experiments, some additional C_1 and small fractions of C_2 and C^* are found for pure cinnamyl alcohol (see Table I). These originate in contaminations due to the preparation by thermal evaporation. The Ar plasma treatment reduces the cinnamyl alcohol molecules, which is indicated by the decrease of carbon-oxygen single bonds (C_1) and an increasing amount carbon that is not bound to oxygen (C_0, see Table II). The fraction of carbon-oxygen double bonds almost does not change.[24] The same behavior has been described previously for lignin.[23] The adsorption of Ag onto cinnamyl alcohol as well as Ar plasma treated cinnamyl alcohol leads to a decrease of the C_0 species for the benefit of C_1, as well as a significant increase of the C^* species. The C_2 species vanishes for Ag on pure cinnamyl alcohol, whereas it increases for Ag on Ar plasma treated cinnamyl alcohol.

The Ag 3d region (b) shows very similar structures for all three silver films. Only one bonding state is visible, the two peaks are due to spin-orbit coupling. The Ag 3d spectra of Ag on Si(100), Ag on cinnamyl alcohol, and Ag on Ar – plasma-treated cinnamyl alcohol are shaped equally. Only one bonding state can be found, the binding energies and FWHM are nearly the same for all three systems (see Table III). These results suggest that only metallic Ag is present after adsorption on pure cinnamyl alcohol as well as on Ag – plasma-treated cinnamyl alcohol and that no chemical interaction occurs between Ag and cinnamyl alcohol as was already supposed during the discussion of the MIES and UPS spectra.

Summarizing the spectroscopic results, we find Ag to remain metal-like on adsorption without being chemically influenced by underlying cinnamyl alcohol. On the other hand, the underlying cinnamyl alcohol film gets slightly oxidized forming additional carbon-oxygen single bonds during the Ag adsorption, independent of a preliminary Ar plasma treatment.

B. Microscopic results

Figure 4 shows AFM images of Ag on Si(100) (a) and Ag on Ar – plasma-treated cinnamyl alcohol (b). The Ag on

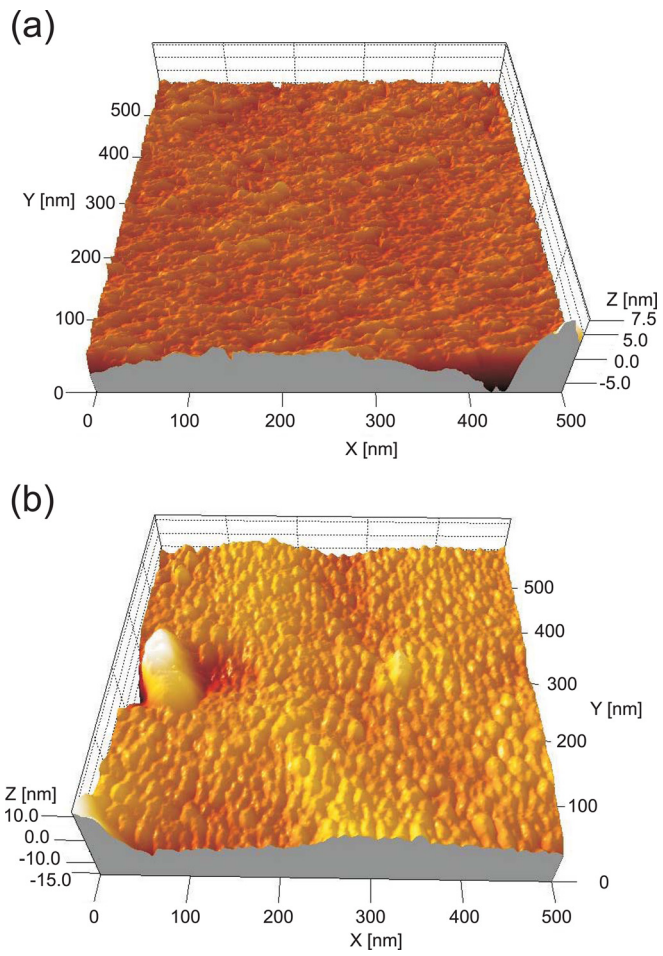

FIG. 4. (Color online) AFM images of Ag on Si(100) (a) and Ag on Ar – plasma-treated cinnamyl alcohol (b).

Si(100) surface (a) is displayed as 3 D image with a size of 500×500 nm^2 and a z-range of 15 nm. It shows an average surface roughness of 0.58 nm calculated as root mean square by SPIP (Image Metrology A/S) after ISO 4287/1 with no particle or island formation visible. Therefore, we assume that a closed Ag film is formed on the Si(100) substrate. This validates the calculation of the growth rate by the attenuation of the Si 2p intensity in XPS, which is based on a closed adlayer.

The Ag coated cinnamyl alcohol surface (b) is displayed as 3 D image with a size of 500×500 nm^2 again, but with a z-range of 30 nm. At the left border, two hillocks with a height around 20 nm and a diameter of about 100 nm are visible, which are believed to be aerosol particles. All over the surface, structures of about 2 nm height appear after the evaporation of Ag on cinnamyl alcohol films (see Fig. 4(b)), thus causing an average surface roughness (the average roughness was calculated as described above) of 1.82 nm. These structures can be interpreted as particles. Since the subjacent pure cinnamyl alcohol did not show any distinct structuring, these periodic bumps indicate the formation of silver nano particles.

Figure 5 shows a statistical evaluation of the number of particles as a function of the nano particles area (a) and as a function of the nano particles maximum length (b) in Fig. 4(b). The particle mean area (A) amounts to 76 nm^2 at a mean maximum length of (13 ± 5) nm and a mean diameter

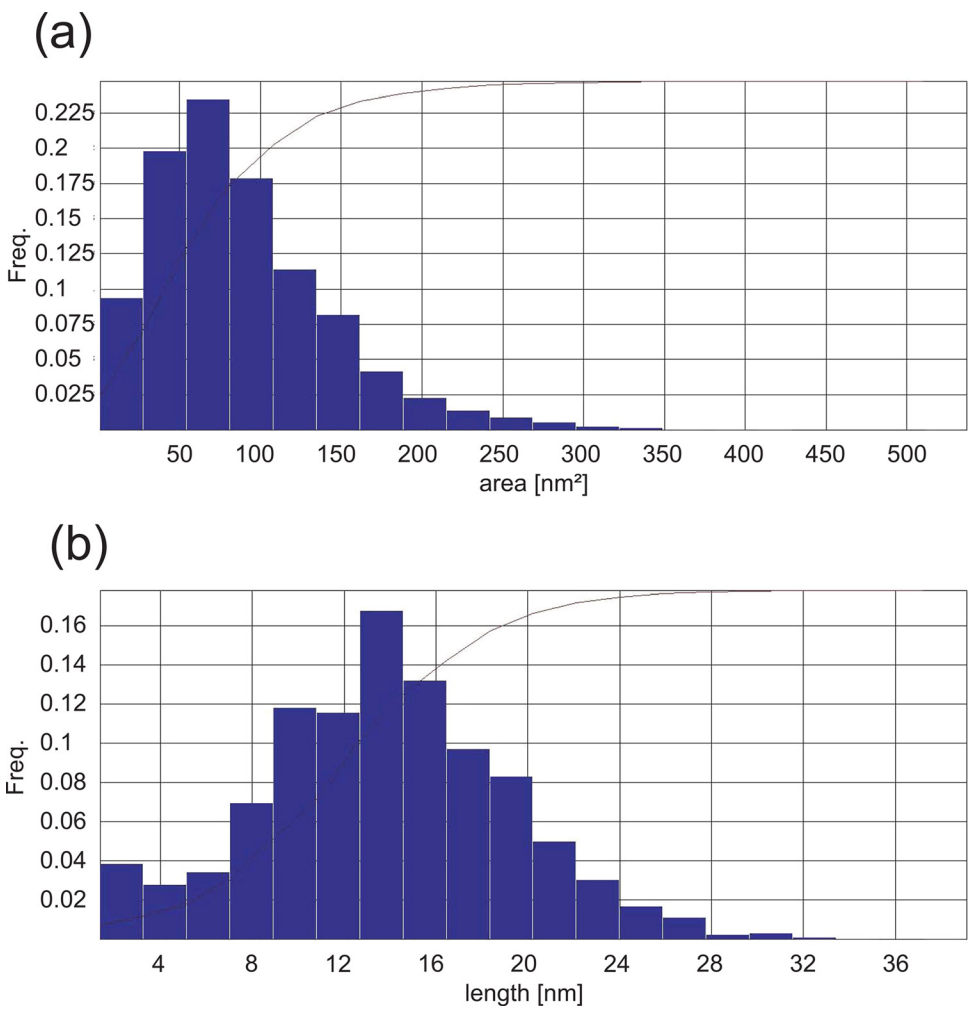

FIG. 5. (Color online) Statistical evaluation of the number of particles as a function of the area each particle covers (a) and as a function of the length of each particle (b) of the Ag nano particles on Ar – plasma-treated cinnamyl alcohol.

($d = 2\sqrt{A/\pi}$) of (9 ± 4) nm. The error values correspond to the respective standard deviation.

These results explain why cinnamyl alcohol structures are weakly visible in UPS but vanish in MIES. Since the experimental setup includes an angle of 45° between the surface and the approaching He^* atoms, the underlying film of cinnamyl alcohol is shaded by the silver particles, thus no signal due to cinnamyl alcohol can be detected in MIES. In contrast to that, UV photons can penetrate the whole silver nano particles, even though the intensity decays to about 20%.[43] Afterwards, the UV photons can excite photoelectrons. These photoelectrons however should not appear in the spectra for all regions below particles, since the intermediate mean free path should be well below 1.5 nm.[44] Therefore, the structures of cinnamyl alcohol that remain in the UPS spectra after adsorption of Ag are believed to originate in the regions of the cinnamyl alcohol film below the gaps between the silver nano particles.

IV. SUMMARY

The adsorption of Ag atoms on films of cinnamyl alcohol leads to the formation of nanoparticles with a mean diameter of about 9 nm as determined by AFM. These particles cover the molecular layer completely and do not penetrate into it. We do not observe any chemical interaction between the Ag adatoms and the underlying cinnamyl alcohol films as was shown by the combination of MIES, UPS, and XPS.

The pretreatment of the cinnamyl film in a dielectric barrier discharge plasma using Ar changes the electronic structures as was investigated previously. OH groups are removed and the surface is reduced. Nevertheless, the subsequent Ag adsorption onto the pretreated cinnamyl film does not change either the Ag particles sizes or the missing chemical reactions. Obviously, the chemical interaction between Ag and cinnamyl film is very weak or negligible even if the surface is reduced by the plasma treatment.

This gives the opportunity to adsorb silver nano particle onto cinnamyl alcohol surfaces during plasma treatment in process gases with reducing character.

ACKNOWLEDGMENTS

We thankfully acknowledge the provision of the atomic force microscope by the group of Professor W. Daum (Institut für Energieforschung und Physikalische Technologien, TU Clausthal) as well as the technical assistance of Dana Schulte Genannt Berthold. Finally, we thank the Deutsche Forschungsgemeinschaft (DFG) for financial support under Project Nos. MA 1893/18-1 and VI 359/9-1.

[1]K. Y. Yang, K. C. Choi, and C. W. Ahn, Opt. Express **17**, 11495 (2009).
[2]S. Kato, Y. Hirano, M. Iwata, T. Sano, K. Takeuchi, and S. Matsuzawa, Appl. Catal. B – Environ. **57**, 109 (2005).
[3]H.-Y. Chuang and D.-H. Chen, Nanotechnology **20**, 105704 (2009).
[4]C.-N. Lok, C.-M. Ho, R. Chen, Q.-Y. He, W.-Y. Yu, H. Sun, P. K. -H.K.-H. Tam, J.-F. Chiu, and C.-M. Che, J. Proteome Res. **5**, 916 (2006).
[5]V. Ilic, Z. Saponjic, V. Vodnic, S. Lazovic, S. Dimitrijevic, P. Jovancic, J. M. Nedeljkovic, and M. Radetic, Ind. Eng. Chem. Res. **49**, 7287 (2010).
[6]P. Rehn and W. Viöl, Holz Roh. Werkst. **61**, pp. 145–150.
[7]P. Rehn, A. Wolkenhauer, M. Bente, S. Förster, and W. Viöl, Surf. Coat. Tech. **174–175**, 515 (2003).
[8]M. Bente, G. Avramidis, S. Förster, E.G. Rohwer, and W. Viöl, Holz Roh. Werkst. **62**, pp. 157–163.
[9]A. Wolkenhauer, A. Meiners, P. Rehn, G. Avramidis, M. Leck, and W. Viöl, Holztechnologie **46**, 40 (2005).
[10]M. Kopp, E. Roddewig, H. Günther, G. Ohms, M. Leck, and W. Viöl, Laser Phys. Lett. **2**, 16 (2005).
[11]A. Wolkenhauer, G. Avramidis, E. Hauswald, H. Militz, and W. Viöl, Int. J. Adhes. Adhes. **29**, 18 (2009).
[12]L. Podgorski, B. Chevet, L. Onic, and A. Merlin, Int. J. Adhes. Adhes. **20**, 103 (2000).
[13]I. Topala and N. Dumitrascu, J. Adhes. Sci. Technol. **21**, 1089 (2007).
[14]M. Odraskova, J. Rahel, A. Zahoranova, R. Tino, and M. Cernak, Plasma Chem. Plasma P. **28**, 203 (2008).
[15]G. Toriz, M. G. Gutierrez, V. Gonzalez-Alvarez, A. Wendel, P. Gatenholm, and A. D. Martinez-Gomez, J. Adhes. Sci. Technol. **22**, 2059 (2008).
[16]M. Asandulesa, I. Topala, and N. Dumitrascu, Holzforschung **64**, 223 (2010).
[17]Y. Liu, Y. Tao, X. Lv, Y. Zhang, and M. Di, Appl. Surf. Sci. **257**, 1112 (2010).
[18]F. Busnel, V. Blanchard, J. Prégent, L. Stafford, B. Riedl, P. Blanchet, and A. Sarkissian, J. Adhes. Sci. Technol. **24**, 1401 (2010).
[19]M. Gindrat, H.-M. Höhle, K. von Niessen, P. Guittienne, D. Grange, and C. Hollenstein, J. Therm. Spray Techn. **20**, 882 (2011).
[20]G. Avramidis, A. Wolkenhauer, B. Zhen, H. Militz, and W. Viöl, ECWM **4**, 269 (2009).
[21]L. Klarhöfer, F. Voigts, D. Schwendt, B. Roos, W. Viöl, O. Höfft, and W. Maus-Friedrichs, Holzforschung **61**, 523 (2007).
[22]L. Klarhöfer, B. Roos, W. Viöl, O. Höfft, S. Dieckhoff, V. Kempter, and W. Maus-Friedrichs, Holzforschung **62**, 688 (2008).
[23]L. Klarhöfer, W. Viöl, and W. Maus-Friedrichs, Holzforschung **64**, 331 (2010).
[24]L. Klarhöfer, °Ph.D. thesis at the Clausthal Technical University, 2009.
[25]T. V. Sorokina, D. Dollimore, and K. S. Alexander, Thermochim. Acta **392–393**, 315 (2002).
[26]S. C. Rastogi, J. D. Johansen, P. Frosch, T. Menné, M. Bruze, J. P. Lepoittevin, B. Dreier, K. E. Andersen, and I. R. White, Contact Dermatitis **38**, 29 (1998).
[27]N. Gupta, S. D. Shenoi, and C. Balachandran, Contact Dermatitis **40**, 53 (1999).
[28]W. G. Larsen, J. Am. Acad. Dermatol. **12**, 1 (1985).
[29]W. Maus-Friedrichs, M. Wehrhahn, S. Dieckhoff, and V. Kempter, Surf. Sci. **249**, 149 (1991).
[30]D. Ochs, W. Maus-Friedrichs, M. Brause, J. Günster, V. Kempter, V. Puchin, A. Shluger, and L. Kantorovich, Surf. Sci. **365**, 557 (1996).
[31]D. Ochs, M. Brause, B. Braun, W. Maus-Friedrichs, and V. Kempter, Surf. Sci. **397**, 101 (1998).
[32]S. Krischok, O. Höfft, J. Günster, J. Stultz, D. W. Goodman, and V. Kempter, Surf. Sci. **495**, 8 (2001).
[33]J. H. Scofield, J. Electron Spectrosc. Relat. Phenom. **8**, 129 (1976).
[34]R. F. Reilman, A. Msezane, and S. T. Manson, J. Electr. Spectr. Rel. Phen. **8**, 389 (1976).
[35]C. Powell and A. Jablonski, J. Electr. Spectr. Rel. Phen. **178**, 331 (2010).
[36]C. J. Powell and A. Jablonski, NIST Electron Inelastic-Mean-Free-Path Database - Version 1.2, National Institute of Standards and Technology, Gaithersburg, MD, 2010, http://www.nist.gov/srd/nist71.cfm.
[37]Y. Harada, S. Masuda, and H. Ozaki, Chem. Rev. **97**, 1897 (1997).
[38]H. Morgner, Adv. At. Mol. Opt. Phys. **42**, 387 (2000).
[39]G. Ertl and J. Kuppers, *Low Energy Electrons and Surface Chemistry* (VCH Verlag, Weinheim, 1985).
[40]L. Wegewitz, S. Dahle, O. Höfft, F. Voigts, W. Viöl, F. Endres, and W. Maus-Friedrichs, J. Appl. Phys. **110**, 033302 (2011).
[41]U. Kogelschatz, Plasma Chem. Plasma P. **23**, 1 (2003).
[42]P. Stracke, S. Krischok, and V. Kempter, Surf. Sci. **473**, 86 (2001).
[43]B. L. Henke, E. M. Gullikson, and J. C. Davis, Atomic Data and Nuclear Data Tables, Vol. **54** (No. 2), 181–342, 1993, http://henke.lbl.gov/optical_constants/.
[44]M. P. Seah and W. A. Dench, Surf. Int. Anal. **1**, 2 (1979).